Improved Gauss-Seidel Projection Method for Micromagnetics Simulations

Carlos J. García-Cervera[*] and Weinan E[†]

Abstract

The *Gauss-Seidel Projection Method* (GSPM), introduced by Wang, Garcia-Cervera, and E in *J. Comp. Phys.*, **171**, pp. 357-372, 2001, is a simple, efficient, and unconditionally stable method for micromagnetics simulations. We present an improvement of the method for small values of the damping parameter. With the new method we are able to carry out fully resolved simulations of the magnetization reversal process in the presence of thermal noise.

1 Introduction

Understanding the mechanisms of magnetization reversal in ferromagnetic samples of nano-scale size is of interest in the study of the magnetic recording process, in particular in computer disks and in computer memory cells, such as MRAMs [1, 2]. Numerical simulation has become an important tool in the study of both static and dynamic issues in ferromagnetic materials [3, 4, 5, 6, 7, 8, 9, 10, 11], and in particular, the magnetization reversal process has been the subject of a large number of experimental studies. Most studies coincide that the presence of magnetization vortices inside a ferromagnetic sample has a dramatic effect in the magnetization reversal process [12, 13, 14, 15, 16]. It is therefore necessary to resolve numerically length scales comparable to the size of magnetic vortices in order to carry out realistic micromagnetics simulations.

[*]Carlos J. García-Cervera is currently at the Mathematics Department, University of California, Santa Barbara, CA 93106. E-mail: cgarcia@math.ucsb.edu. URL: http://www.math.ucsb.edu/~cgarcia.

[†]Weinan E is currently at the Mathematics Department and Program in Applied and Computational Mathematics, Princeton University, NJ 08540. E-mail: weinan@princeton.edu. URL: http://www.math.princeton.edu/~weinan.

The Landau-Lifshitz equation [17, 18],

$$\mathbf{M}_t = -\mu_0\gamma\mathbf{M}\times\mathcal{H} - \frac{\mu_0\gamma\alpha}{M_s}\mathbf{M}\times(\mathbf{M}\times\mathcal{H}) \tag{1}$$

describes the relaxation process of the magnetization in a ferromagnetic material. In (1), $|\mathbf{M}| = M_s$ is the saturation magnetization, and is usually set to be a constant far from the Curie temperature, and μ_0 is the permeability of vacuum ($\mu_0 = 4\pi\times 10^{-7}N/A^2$ in the S.I.). The first term on the right hand side is the gyromagnetic term, with γ being the gyromagnetic ratio. The second term in the right hand side is the damping term, with α being the dimensionless damping coefficient. $\mathcal{H}$ is the local field,

$$\mathcal{H} = \frac{A}{\mu_0 M_s^2}\Delta\mathbf{M} + \frac{1}{\mu_0 M_s}w\left(\frac{\mathbf{M}}{M_s}\right) + \mathbf{H}_e - \nabla U. \tag{2}$$

In (2), A is the exchange constant, $\frac{A}{M_s^2}\Delta\mathbf{M}$ is the exchange interaction between the spins, $\frac{1}{M_s}w\left(\frac{\mathbf{M}}{M_s}\right)$ is the field due to material anisotropy, $\mathbf{H}_e$ is the external applied field, Ω is the volume occupied by the material, and finally the last term in (2) is the field induced by the magnetization distribution inside the material. This induced field $\mathbf{H}_s = -\nabla U$ can be computed by solving:

$$\Delta U = \begin{cases} \nabla\cdot\mathbf{M} & \text{in } \Omega \\ 0 & \text{outside } \Omega \end{cases} \tag{3}$$

together with the jump conditions

$$\begin{aligned} [U]_{\partial\Omega} &= 0 \\ \left[\frac{\partial U}{\partial\nu}\right]_{\partial\Omega} &= -\mathbf{M}\cdot\nu \end{aligned} \tag{4}$$

at the boundary of the domain Ω. In (4) we denote by $[v]_{\partial\Omega}$ the jump of v at boundary of Ω:

$$[v]_{|\partial\Omega}(x) = \lim_{\substack{y\to x \\ y\in\bar{\Omega}^c}} v(y) - \lim_{\substack{y\to x \\ y\in\Omega}} v(y)$$

Currently, the most commonly used methods for the simulation of the Landau-Lifshitz equation are explicit numerical schemes, such as fourth order Runge-Kutta, or predictor-corrector schemes, with some kind of adaptive time stepping procedure. Although explicit schemes may achieve high order of accuracy both in space and time, the time step size is severely constrained by

the stability of the numerical scheme. For physical constants characteristic of the permalloy ($M_s = 8.0 \times 10^5$ Ampere$/m$, $K_u = 5.0 \times 10^2$ J/m^3, $A = 1.3 \times 10^{-11}$ J/m, $\gamma = 1.76 \times 10^{11}$ $T^{-1}s^{-1}$), with a cell size $\Delta x = 0.004\,\mu m$ (256 grid points in a $1\,\mu m$ long sample), and using fourth order Runge-Kutta, we need to use a time step roughly of the order $\Delta t \approx .25$ picoseconds for numerical stability. If the cell size is decreased by a factor of 10, the time step Δt must be reduced by a factor of 100. This time step restriction is even more severe when considering the stochastic Landau-Lifshitz equations with Langevin dynamics. In such case, with a cell size $\Delta x = 0.006\,\mu m$, a time step $\Delta t \approx 0.1$ femtoseconds is needed [19, 20].

A simple, efficient, and unconditionally stable scheme for (1), the *Gauss-Seidel Projection Method* (GSPM), was introduced by Wang, Garcia-Cervera, and E in [21]. With this method, we were able to carry out fully resolved calculations for the switching of the magnetization in micron-size elements. The same method has been used by Wang, Wang, and E to study the dependence of the switching field on film thickness, and the structure of cross-tie walls [22].

The time step size necessary for numerical stability of the GSPM was found to be independent of the spatial grid size. However, a dependence on the damping parameter α was pointed out by M. Scheinfein [23]. For $\alpha = 0.1$, one can perform accurate simulations with $\Delta t = 1$ picosecond. For $\alpha = 0.01$, one needs to use a time step size 10 times smaller. In this article we present an improvement of the GSPM which allows us to use a time step $\Delta t = 2$ picoseconds with $\alpha = 0.001$. With the new method we have been able to carry out fully resolved simulations of the stochastic Landau-Lifshitz equations, with time step size $\Delta t = 1$ picosecond, for a cell size $\Delta x = 0.004\,\mu m$.

The rest of the paper is organized as follows: In Section 2 we describe the main ideas behind the GSPM. A more detailed description can be found in [21]. The improved GSPM is presented in Section 3. Finally, some numerical results are presented in Section 4.

2 The Gauss-Seidel Projection Method

In order to illustrate the main ideas behind the GSPM, let us consider first the case when only the exchange term is kept in (2). For clarity, all the constants are ignored. In this case $\mathcal{H} = \Delta \mathbf{m}$ and the Landau-Lifshitz equation (1) reduces to

$$\mathbf{m}_t = -\mathbf{m} \times \Delta \mathbf{m} - \mathbf{m} \times (\mathbf{m} \times \Delta \mathbf{m}) \tag{5}$$

In order to overcome the stability constraint of explicit schemes, one usually resorts to implicit schemes [8]. However, due to the strong nonlinearities present in both the gyromagnetic and damping terms in the Landau-Lifshitz equation (1), a direct implicit discretization of the system is not efficient and is difficult to implement.

When only the damping term is present, equation (5) becomes

$$\mathbf{m}_t = -\mathbf{m} \times (\mathbf{m} \times \Delta \mathbf{m}) = \Delta \mathbf{m} + |\nabla \mathbf{m}|^2 \mathbf{m} \tag{6}$$

A simple projection scheme for this equation was introduced by E and Wang [24]. This scheme was shown to be unconditionally stable and more efficient than other schemes used for the simulation of equation (6).

The focus in [21] was the gyromagnetic term in the Landau-Lifshitz equation:

$$\mathbf{m}_t = -\mathbf{m} \times \Delta \mathbf{m} \tag{7}$$

To overcome the nonlinearity of the equation, consider the following simple fractional step scheme

$$\begin{aligned} \frac{\mathbf{m}^* - \mathbf{m}^n}{\Delta t} &= \Delta_h \mathbf{m}^* \\ \mathbf{m}^{n+1} &= \mathbf{m}^n - \mathbf{m}^n \times \mathbf{m}^* \end{aligned} \tag{8}$$

The advantage of the scheme (8) is that the implicit step is now linear, comparable to solving heat equations implicitly, and is easy to implement. It is easy to check that the scheme (8) is consistent with (7) and is first order accurate in time. However, direct numerical implementation of (8) shows that the scheme is unstable. The main idea in the GSPM is to use a Gauss-Seidel type of technique, to improve the stability properties of (8). Let

$$g_i^n = (I - \Delta t \Delta_h)^{-1} m_i^n, \qquad i = 1, 2, 3 \tag{9}$$

The update in the GSPM is defined as follows

$$\begin{pmatrix} m_1^{n+1} \\ m_2^{n+1} \\ m_3^{n+1} \end{pmatrix} = \begin{pmatrix} m_1^n + (g_2^n m_3^n - g_3^n m_2^n) \\ m_2^n + (g_3^n m_1^{n+1} - g_1^{n+1} m_3^n) \\ m_3^n + (g_1^{n+1} m_2^{n+1} - g_2^{n+1} m_1^{n+1}) \end{pmatrix} \tag{10}$$

Note that the newly updated value m_1^{n+1} is used to compute m_2^{n+1}, and these two new values are used to update m_3.

3 Improved Gauss-Seidel projection scheme for the full Landau-Lifshitz Equation

For the full Landau-Lifshitz equation (1), we couple the above implicit Gauss-Seidel scheme with the projection method developed earlier in [24], in a fractional step framework. Since $\mathbf{M}$ and $\mathcal{H}$ have the same physical dimensions, we can write $\mathcal{H} = M_s\mathbf{h}$, $\mathbf{H}_s = M_s\mathbf{h}_s$, $\mathbf{H}_e = M_s\mathbf{h}_e$, and $\mathbf{M} = M_s\mathbf{m}$. Without loss of generality, we will assume that the material is uniaxial, and $w(\mathbf{m}) = -\frac{K_u}{M_s}(m_2\mathbf{e}_2 + m_3\mathbf{e}_3)$, where $\mathbf{e}_1 = (1,0,0)$, $\mathbf{e}_2 = (0,1,0)$, and $\mathbf{e}_3 = (0,0,1)$. Equation (1) is rewritten as:

$$\mathbf{m}_t = -\mu_0\gamma M_s\ \mathbf{m}\times\mathbf{h} - \mu_0\gamma M_s\alpha\ \mathbf{m}\times\mathbf{m}\times\mathbf{h} \tag{11}$$

where

$$\mathbf{h} = -\frac{K_u}{\mu_0 M_s^2}(m_2\mathbf{e}_2 + m_3\mathbf{e}_3) + \frac{A}{\mu_0 M_s^2}\Delta\mathbf{m} + \mathbf{h}_s + \mathbf{h}_e \tag{12}$$

The constant $\mu_0\gamma M_s$ has dimensions of the reciprocal of time (s^{-1}). Therefore we rescale in time: $t \to (\mu_0\gamma M_s)^{-1}\,t$, and we rescale the spatial variable $x \to Lx$ where L is the diameter of Ω. The equation becomes:

$$\mathbf{m}_t = -\mathbf{m}\times\mathbf{h} - \alpha\,\mathbf{m}\times\mathbf{m}\times\mathbf{h} \tag{13}$$

where

$$\mathbf{h} = -Q(m_2\mathbf{e}_2 + m_3\mathbf{e}_3) + \epsilon\Delta\mathbf{m} + \mathbf{h}_s + \mathbf{h}_e \tag{14}$$

Here we have defined the dimensionless parameters $Q = K_u/(\mu_0 M_s^2)$, and $\epsilon = A/(\mu_0 M_s^2 L^2)$.

For our splitting procedure, we define the vector field:

$$\mathbf{f} = -Q(m_2\mathbf{e}_2 + m_3\mathbf{e}_3) + \mathbf{h}_s + \mathbf{h}_e \tag{15}$$

We solve equation

$$\mathbf{m}_t = -\mathbf{m}\times(\epsilon\Delta\mathbf{m} + \mathbf{f}) - \alpha\,\mathbf{m}\times\mathbf{m}\times(\epsilon\Delta\mathbf{m} + \mathbf{f}) \tag{16}$$

in three steps:
Step 1: Implicit Gauss-Seidel.

$$\begin{aligned} g_i^n &= (I - \epsilon\Delta t\Delta_h)^{-1}(m_i^n + \Delta t f_i^n), \\ g_i^* &= (I - \epsilon\Delta t\Delta_h)^{-1}(m_i^* + \Delta t f_i^*), \qquad i = 1,2,3 \end{aligned} \tag{17}$$

$$\begin{pmatrix} m_1^* \\ m_2^* \\ m_3^* \end{pmatrix} = \begin{pmatrix} m_1^n + (g_2^n m_3^n - g_3^n m_2^n) \\ m_2^n + (g_3^n m_1^* - g_1^* m_3^n) \\ m_3^n + (g_1^* m_2^* - g_2^* m_1^*) \end{pmatrix} \tag{18}$$

Step 2: Heat flow without constraints.

$$\mathbf{f}^* = -Q\,(m_2^* \mathbf{e}_2 + m_3^* \mathbf{e}_3) + \mathbf{h}_s^* + \mathbf{h}_e \tag{19}$$

$$\begin{pmatrix} m_1^{**} \\ m_2^{**} \\ m_3^{**} \end{pmatrix} = \begin{pmatrix} m_1^* + \alpha \Delta t(\epsilon \Delta_h m_1^{**} + f_1^*) \\ m_2^* + \alpha \Delta t(\epsilon \Delta_h m_2^{**} + f_2^*) \\ m_3^* + \alpha \Delta t(\epsilon \Delta_h m_3^{**} + f_3^*) \end{pmatrix} \tag{20}$$

Step 3: Projection onto S^2.

$$\begin{pmatrix} m_1^{n+1} \\ m_2^{n+1} \\ m_3^{n+1} \end{pmatrix} = \frac{1}{|m^{**}|} \begin{pmatrix} m_1^{**} \\ m_2^{**} \\ m_3^{**} \end{pmatrix} \tag{21}$$

Note that the stray field is recomputed using the intermediate values of $\mathbf{m}$ in (17), and (19). In the original implementation of the GSPM [21], the stray field was not recomputed using these intermediate values. Instead, the value $\mathbf{h}_s^n$ was used in (17), and (19).

4 Numerical Results

To illustrate the improved properties of the new GSPM, we have carried out fully resolved simulations of the full Landau-Lifshitz equations (1). In our first simulation, we simply illustrate the deficiency of the original GSPM by presenting the results obtained with the original GSPM for $\alpha = 0.01$. In our second simulation, we have considered the stochastic Landau-Lifshitz equation with Langevin dynamics and simulated the magnetization reversal process at room temperature.

In our implementation of the GSPM, we divided the computational domain into cells. In each cell we approximated the magnetization by a vector with constant magnitude, but free to rotate in any direction. We approximated the stray field by its average value in each cell. This stray field was computed using Fast Fourier Transform (FFT). The Helmholtz-type equations that appear in steps 1 and 2 of the GSPM were solved via an FFT-based Fast Poisson Solver.

The results of our first experiment are shown in Fig. 1. We compare the results obtained using the old GSPM for two different values of the damping parameter, $\alpha = 0.1$ and $\alpha = 0.01$, and without an applied field. For both

simulations we considered a time step size $\Delta t = 1$ picosecond and a cell size $\Delta x = 0.004\,\mu m$. The initial state was fully saturated, and the sample was let to relax without external field. The results for $\alpha = 0.1$ are presented on the left column, and the results for $\alpha = 0.01$ are presented on the right column. We present in figures 1.(a) and 1.(c) a grey scale plot of the angle between the in-plane magnetization and the OX axis. In figures 1.(b) and 1.(d) we plot the actual in-plane magnetization field that corresponds to 1.(a) and 1.(c), respectively. The results obtained with the old GSPM for $\alpha = 0.01$ suffer a complete loss of accuracy. A time step size $\Delta t = 0.1$ picoseconds was needed to obtain accurate results. This time step size was found to be independent of the spatial grid size, confirming the unconditional stability properties of the numerical scheme.

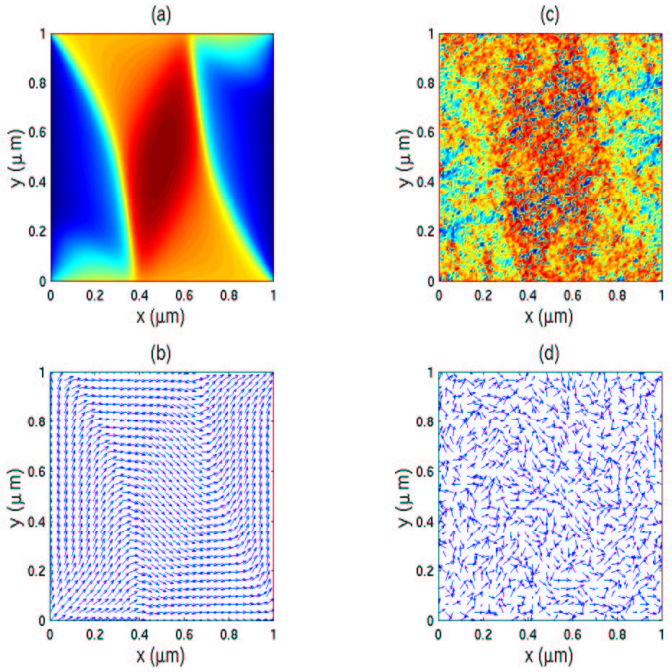

Figure 1: Simulation of the full Landau-Lifshitz equations using the old GSPM. Left column: $\alpha = 0.1$. Right column: $\alpha = 0.01$. For both simulations, $\Delta x = 0.004\,\mu m$, and $\Delta t = 1$ picosecond.

For our second experiment, we considered the Landau-Lifshitz equation

with stochastic forcing. The Langevin dynamical equations are

$$\mathbf{M}_t = -\mu_0\gamma\mathbf{M}\times\left(\mathcal{H}+\dot{\mathcal{W}}(t)\right) - \frac{\mu_0\gamma\alpha}{M_s}\mathbf{M}\times\left(\mathbf{M}\times\left(\mathcal{H}+\dot{\mathcal{W}}(t)\right)\right). \quad (22)$$

In (22), $\dot{\mathcal{W}}$ represents the effect of thermal fluctuations, and it is uncorrelated, independent, Gaussian white noise, characterized by the moments

$$\begin{aligned} \left\langle \dot{\mathcal{W}}_i(t)\right\rangle &= 0, \\ \left\langle \dot{\mathcal{W}}_i^j(t)\dot{\mathcal{W}}_k^l(t')\right\rangle &= \frac{2\alpha k_B T}{\mu_0^2\gamma M_s}\delta_{ik}\delta_{jl}\delta(t-t'). \end{aligned} \quad (23)$$

In (23), $\langle v\rangle$ represents the expected value of the random variable v; k_B is the Boltzmann constant ($k_B = 1.38054\times 10^{-23}$ Joules/degree), T is the absolute temperature, and γ is the gyromagnetic ratio. The subindices in $\dot{\mathcal{W}}$ represent different spatial locations, and the superindices represent each vector component of $\dot{\mathcal{W}}$.

The effect of vortices in the magnetization reversal process has been studied thoroughly in the past few years [16, 14, 25]. In the experiments presented in [25], the nucleation of vortices was observed during the reversal process. These vortices facilitated the growth of magnetic domains with increasing fields, and disappeared after the reversal was complete. The vortex state was found to be stable, in the sense that the sample stayed in the vortex state for a wide range of external fields. In the numerical experiments performed in [25], the magnetization reversal always occurred by vortex nucleation. However, the vortices only appeared momentarily at the switching field. For a sample of dimensions $1\,\mu m\times 0.2\,\mu m\times 300\,\text{Å}$, this field was found to be 190 Oe experimentally, and 900 Oe numerically.

The results at room temperature ($T = 300K$), for several values of the damping parameter α, are shown in figures 2 and 3. In all cases, we were able to compute the hysteresis loop using a time step size $\Delta t = 1$ picosecond, for a cell size $\Delta x = 0.004\,\mu m$. For comparison, note that the numerical integration of the stochastic Landau-Lifshitz equation using the Heun method, for a cell size $\Delta x = 0.006\,\mu m$, requires a time step size $\Delta t \approx 0.1$ femtoseconds [19, 20]. Our method provides an improvement of approximately four orders of magnitude in the time step size required.

In our simulations, we considered a permalloy sample with dimensions $1\,\mu m\times 0.2\,\mu m\times 300\,\text{Å}$. A positive external field was applied to obtain the metastable state shown in figure 3.(a), frequently known as S state. The hysteresis loop was calculated quasi statically. Starting from a value $H_e = 0$ Oe, the applied field was decreased in steps of 4 Oe when equilibrium

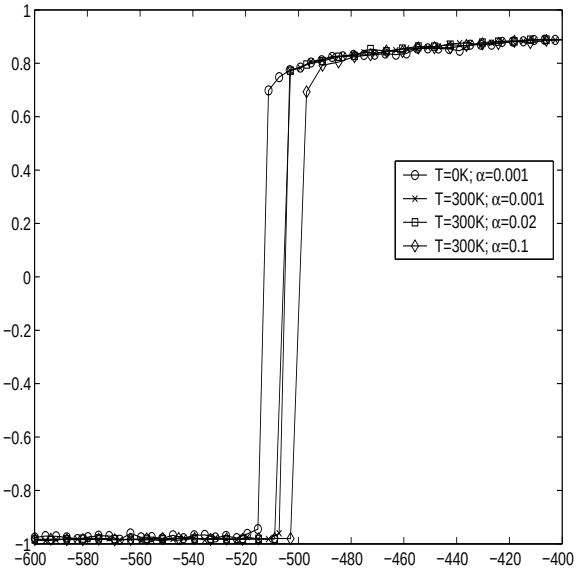

Figure 2: Comparison of hysteresis loops at zero temperature and at room temperature, for several values of the damping parameter α. The switching field is approximately -515 Oe at zero temperature. At room temperature, the reversal occurred at -507 Oe for $\alpha = 0.001$ and $\alpha = 0.02$, and at -503 for $\alpha = 0.1$.

was reached. At zero temperature, two criteria were used to determine that a steady state had been reached: either the simulation had run for 10 nanoseconds, or the relative change in the average magnetization after 10 steps was less than 10^{-6}. At room temperature, the simulation was run for 10 nanoseconds for each different field.

Our results are consistent with the numerical simulations presented in [25]. The magnetization reversal occurred by vortex nucleation: a couple of vortices appeared near the end domains, and they moved quickly, reversing the magnetization. The vortices only appeared momentarily at the switching field. The switching field obtained in our computations at zero temperature was about $\mathbf{H}_c = -515(\pm 4)$ Oe. At room temperature, the reversal occurred at about $\mathbf{H}_c = -507(\pm 4)$ Oe. This small change in the switching field seems to indicate that thermal effects are not responsible for the nucleation of these vortices.

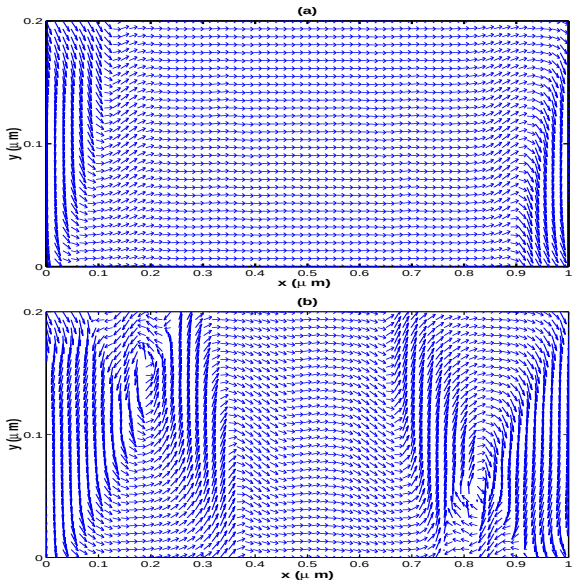

Figure 3: Two stages during the magnetization reversal process in a sample of dimensions $1\,\mu m \times 0.2\,\mu m \times 300\,\text{Å}$, at room temperature. (a) S state, characterized by a uniform magnetization in the longitudinal direction, with parallel transverse end domains. (b) Nucleation of vortices near the end domains. The nucleation field is about -515 Oe.

5 Conclusions

In conclusion, we have introduced a simple modification to the Gauss Seidel Projection Method, which enhances the accuracy and stability properties of the original method. The new method allows us to perform fully resolved micromagnetics simulations in the presence of thermal noise, with realistic values of the damping constant, with a large time step size.

6 Acknowledgments

We thank Michael Scheinfein for pointing out the problem of the original GSPM to us. We also thank Anthony Arrott, and Roger Koch for helpful discussions. The work of Weinan E was supported in part by NSF, Grant DMS01-30107.

References

[1] J. Daughton. Magnetoresistive memory technology. *Thin Solid Films*, 216:162–168, 1992.

[2] G. Prinz. Magnetoelectronics. *Science*, 282:1660, 1998.

[3] H.N. Bertram and C. Seberino. Numerical simulations of hysteresis in longitudinal magnetic tape. *J. Magn. Magn. Mater.*, 193:388–394, 1999.

[4] J.L. Blue and M.R. Scheinfein. Using multipoles decreases computation time for magnetic self-energy. *IEEE Trans. Magn.*, 27:4778–4780, 1991.

[5] J. Fidler and T. Schrefl. Micromagnetic modelling - the current state of the art. *J. Phys. D: Appl. Phys.*, 33:R135–R156, 2000.

[6] R. Hertel and H. Kronmüller. Adaptive finite element techniques in three-dimensional micromagnetic modeling. *IEEE Trans. Magn.*, 34:3922–3930, 1998.

[7] M. Jones and J.J. Miles. An accurate and efficient 3D micromagnetic simulation of metal evaporated tape. *J. Magn. Magn. Mater.*, 171:190–208, 1997.

[8] Y. Nakatani, Y. Uesake, and N. Hayashi. Direct solution of the Landau-Lifshitz-Gilbert equation for micromagnetics. *Japanese Journal of Applied Physics*, 28(12):2485–2507, 1989.

[9] Y. Nakatani, Y. Uesake, N. Hayashi, and H. Fukushima. Computer simulation of thermal fluctuation of fine particle magnetization based on Langevin equation. *J. Magn. Magn. Mater.*, 168:347–351, 1997.

[10] W. Rave, S. Zielke, and A. Hubert. The magnetic ground state of a thin-film element. *Preprint 61/1999 of MPI-MIS Leipzig, www.mis.mpg.de (submitted to IEEE Trans. Magnetics).*

[11] Samuel W. Yuan and Neal Bertram. Fast adaptive algorithms for micromagnetics. *IEEE Transactions on Magnetics*, 28(5):2031–2036, 1992.

[12] A.F. Popkov, L.L. Savchenko, N.V. Vorotnikova, S. Tehrani, and J. Shi. Edge pinning effect in single- and three-layer patterns. *Applied Physics Letters*, 77(2):277–279, 2000.

[13] J. Shi and S. Tehrani. Edge pinned states in patterned submicron NiFeCo structures. *Applied Physics Letters*, 77(11):1692–1694, 2000.

[14] J. Shi, S. Tehrani, and M.R. Scheinfein. Geometry dependence of magnetization vortices in patterned submicron NiFe elements. *Applied Physics Letters*, 76:2588–2590, 2000.

[15] J. Shi, T. Zhu, M. Durlam, E. Chen, S. Tehrani, Y.F. Zheng, and J.-G. Zhu. End domain states and magnetization reversal in submicron magnetic structures. *IEEE Transactions on Magnetics*, 34:997–999, 1998.

[16] J. Shi, T. Zhu, S. Tehrani, Y.F. Zheng, and J.-G. Zhu. Magnetization vortices and anomalous switching in patterned NiFeCo submicron arrays. *Applied Physics Letters*, 74:2525–2527, 1999.

[17] W.F. Brown Jr. *Micromagnetics*. Interscience Tracts on Physics and Astronomy. Interscience Publishers (John Wiley and Sons), New York - London, 1963.

[18] L. Landau and E. Lifshitz. On the theory of the dispersion of magnetic permeability in ferromagnetic bodies. *Physikalische Zeitschrift der Sowjetunion*, 8:153–169, 1935.

[19] Peter E. Kloeden and Eckhard Platen. *Numerical Solution of Stochastic Differential Equations*. Applications of MAthematics, Vol. 23. Springer-Verlag, Berlin-New York, 1992.

[20] T. Schrefl, W. Scholz, D. Süs, and J. Fidler. Langevin micromagnetics of recording media using subgrain discretization. *IEEE Trans. Mag.*, 36:3189–3191, 2000.

[21] Xiao-Ping Wang, Carlos J. García Cervera, and Weinan E. A Gauss-Seidel Projection Method for the Landau-Lifshitz equation. *J. Comp. Phys.*, 171:357–372, 2001.

[22] Ke Wang, X.P. Wang, and Weinan E. Simulation of 3D micromagnetic structures. *To appear*, 2002.

[23] M. Scheinfein. Personal comunication.

[24] Weinan E and X.P. Wang. Numerical methods for the Landau-Lifshitz equation. *SIAM J. Numer. Anal.*, 38(5):1647–1665, 2000.

[25] K.J. Kirk, M.R. Scheinfein, J.N. Chapman, S. McVitie, M.F. Gillies, B.R. Ward, and J.G. Tennant. Role of vortices in magnetization reversal of rectangular NiFe elements. *J. Phys. D: Appl. Phys.*, 34:160–166, 2001.